

PROGRESS IN THE SURFACE PASSIVATION OF SILICON SOLAR CELLS

Jan Schmidt,¹ Agnes Merkle,¹ Robert Bock,¹ Pietro P. Altermatt,^{1,2} Andres Cuevas,³
Nils-Peter Harder,¹ Bram Hoex,⁴ Richard van de Sanden,⁴ Erwin Kessels,⁴ Rolf Brendel¹

¹Institute for Solar Energy Research Hameln (ISFH), Am Ohrberg 1, 31860 Emmerthal, Germany

²Department of Solid-State Physics, Leibniz University Hanover, Appelstr. 2, 30167 Hanover, Germany

³Department of Engineering, Australian National University, Canberra ACT 0200, Australia

⁴Department of Applied Physics, Eindhoven University of Technology, 5600 MB Eindhoven, The Netherlands

ABSTRACT: In order to increase the efficiency of silicon-wafer-based solar cells in production well above 20%, it is indispensable to improve the currently applied level of surface passivation at the front as well as at the rear of the cells. This paper focuses on two main challenges: (i) the low-temperature passivation of lowly doped *p*-type silicon surfaces at the cell rear and (ii) the passivation of highly boron-doped *p*⁺ emitter surfaces as used at the front of solar cells on high-lifetime *n*-type silicon wafers. In the past, low surface recombination velocities (< 20 cm/s) have been achieved on low-resistivity (~1 Ωcm) *p*-type silicon using plasma-enhanced chemical vapour-deposited (PECVD) silicon nitride (SiN_x) as well as amorphous silicon (a-Si). However, the high density of fixed positive charges within the PECVD-SiN_x layer induces an inversion layer at the rear of *p*-type Si cells, producing a detrimental parasitic shunting, which reduces the short-circuit current density by up to 3 mA/cm². The passivation quality of a-Si on the other hand is very temperature sensitive. More recently it has been shown that atomic-layer-deposited (ALD) aluminium oxide (Al₂O₃) provides an outstanding level of surface passivation, which can be attributed to its extremely high *negative* fixed charge density in combination with the very gentle deposition technique ALD, leading to low interface state densities. The application of these ALD-Al₂O₃ layers to the rear of *p*-type solar cells shows that this new passivation scheme is indeed suitable for high efficiencies and that due to the large negative fixed charge density no parasitic shunting occurs. We also demonstrate that ALD-Al₂O₃ seems to be the ideal passivation layer for boron-doped *p*⁺ emitter surfaces. In a direct comparison with other passivation schemes, it is found that Al₂O₃ even outperforms optimized thermally grown SiO₂ and opens the possibility of achieving very large open-circuit voltages up to $V_{oc} = 740$ mV.

Keywords: Silicon, Surface Passivation, Al₂O₃

1 INTRODUCTION

In high-efficiency laboratory silicon solar cells, surface recombination is very effectively suppressed by means of silicon dioxide (SiO₂) grown in a high-temperature (≥ 900 °C) oxidation process [1]. Very low surface recombination velocities (SRVs) are in particular realized at the lightly doped rear surface, where the combination of a thermally grown SiO₂ layer with an evaporated film of Al give – after an additional annealing treatment at ~400°C (the so-called ‘alneal’) – SRVs below 20 cm/s on un-metallized low-resistivity (~1 Ωcm) *p*-type silicon wafers [2]. In addition, the SiO₂/Al stack at the cell rear acts as an excellent reflector for near-bandgap photons, significantly improving the light trapping properties and hence the short-circuit current of the cell. One of the main reasons why high-temperature oxidation has not been implemented into the majority of industrial cell processes up to now is the high sensitivity of the silicon bulk lifetime to high-temperature processes. In particular in the case of multi-crystalline silicon wafers, thermal processes above 900°C typically lead to a significant degradation of the bulk lifetime [3]. Hence, low-temperature surface passivation alternatives are required for future industrial high-efficiency silicon solar cells, which should have comparable properties as the alnealed SiO₂.

One intensively investigated low-temperature surface passivation alternative to thermal oxide is silicon nitride (SiN_x) grown by plasma-enhanced chemical vapor deposition (PECVD) at ~400°C, which has proven to give comparably low SRVs as thermal SiO₂ on low-resistivity

p-type silicon [4,5]. However, when applied to the rear of PERC (Passivated Emitter and Rear Cell)-type solar cells the short-circuit current density is strongly reduced compared to the SiO₂-passivated cell rear [6]. This effect has been attributed to the large density of fixed positive charges within the SiN_x layer, inducing an inversion layer in the crystalline silicon underneath the SiN_x. The coupling of this inversion layer to the base contact leads to a significant loss in the short-circuit current density. This detrimental effect is known as ‘parasitic shunting’ [7]. Another alternative low-temperature passivation scheme resulting in comparable SRVs as alnealed SiO₂ is intrinsic hydrogenated amorphous silicon (a-Si) deposited by PECVD in the temperature range between 200 and 250°C [8]. Despite the fact that no parasitic shunting occurs in the case of an a-Si passivated cell rear, new problems arise from the high sensitivity of the a-Si passivation to thermal processes. More recently it was shown that thin films of aluminium oxide (Al₂O₃) grown by atomic layer deposition (ALD) provide an excellent level of surface passivation on lowly doped (~1 Ωcm) *p*- and *n*-type silicon wafers [9,10,11] as well as on highly boron-doped *p*⁺ emitters [12].

In the first part of this contribution, we compare the passivation properties of SiN_x, a-Si and ALD-Al₂O₃ regarding the application to the rear of high-efficiency *p*-type silicon solar cells. The second part of the paper addresses the issue of passivating highly boron-doped *p*⁺-emitters, which has been a main obstacle in the past for fabricating high-efficiency cells on high-lifetime *n*-type silicon wafers.

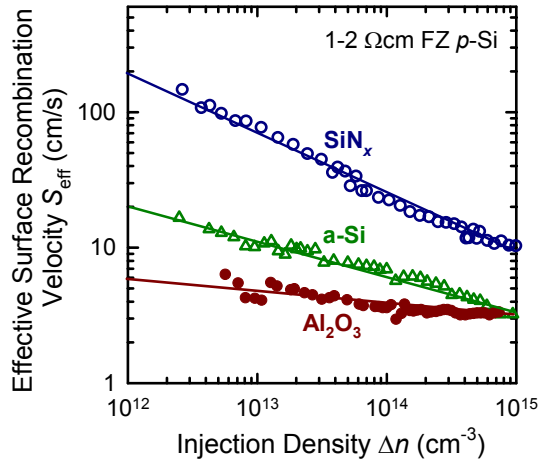
2 PASSIVATION OF UNDIFFUSED *p*-Si


Figure 1. Comparison of the injection-dependent effective SRVs $S_{\text{eff}}(\Delta n)$ measured on 1-2 Ωcm *p*-type float-zone silicon wafers passivated by (i) SiN_x deposited by remote-PECVD [13], (ii) intrinsic a-Si deposited in a parallel-plate PECVD reactor [8] and (iii) Al_2O_3 deposited by means of plasma-assisted ALD [14]. The lines are guides to the eye.

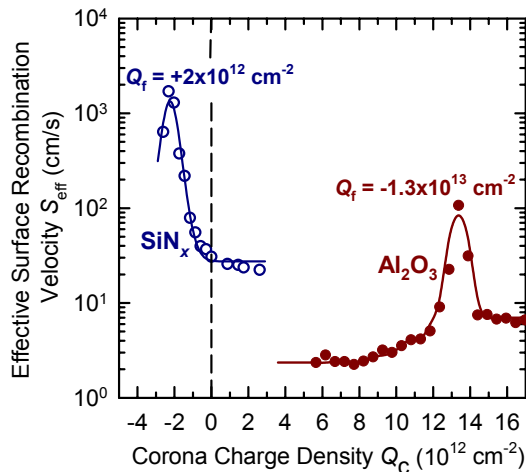


Figure 2. Measured effective SRV S_{eff} as a function of the Corona charge density Q_C deposited onto dielectric passivation layers of SiN_x and Al_2O_3 . The lines are guides to the eye.

Figure 1 shows a comparison of the injection-dependent effective SRVs measured on 1-2 Ωcm *p*-type silicon wafers passivated by (i) SiN_x deposited by remote-PECVD [13], (ii) intrinsic a-Si deposited in a parallel-plate PECVD reactor [8], and (iii) Al_2O_3 deposited by means of plasma-assisted ALD [14]. The measurements are shown in the injection range between 10^{12} and 10^{15} cm^{-3} , which is the most relevant range for the rear of one-sun silicon solar cells. Within this injection range it becomes obvious from Fig. 1 that the Al_2O_3 passivation outperforms the well-optimized SiN_x as well as the a-Si passivation. Importantly, the Al_2O_3 passivation results in a very weak injection level dependence in the injection range between 10^{12} and 10^{15} cm^{-3} , and the effective SRV stays well below 10 cm/s even at low injection densities $< 10^{13}$ cm^{-3} . The strong injection level dependence of the

effective SRV measured on SiN_x -passivated *p*-Si surfaces can be attributed to recombination within the space charge region induced by the high fixed positive charge density within the SiN_x layer [5]. Note that in the past surface recombination velocities down to ~ 200 cm/s had already been achieved by Al_2O_3 films on 1-2 Ωcm *p*-type silicon deposited by atmospheric-pressure chemical vapour deposition [15].

Figure 2 shows the measured effective SRV as a function of the Corona charge density deposited onto dielectric passivation layers of SiN_x and Al_2O_3 . In the flat-band case when the deposited Corona charge density equals the fixed charge density within the dielectric layer, the recombination rate shows a maximum. From this maximum the charge density within the layer can be deduced. As can be seen from Fig. 2, the fixed charge density within the SiN_x layer is positive and amounts to $Q_f = +2 \times 10^{12}$ elementary charges/ cm^2 , whereas the fixed charge density within the Al_2O_3 layer is negative and amounts to $Q_f = -1.3 \times 10^{13}$ cm^{-2} . The fixed negative charge density within the Al_2O_3 layer induces an accumulation layer at the *p*-type silicon surface in contrast to the SiN_x layer inducing an inversion layer. As a consequence, the Al_2O_3 provides a very effective field-effect passivation without the additional contribution of recombination in the space charge region, which is the dominant recombination channel in the case of the SiN_x passivation of *p*-type silicon surfaces at low injection densities [5]. In addition, due to the formation of an accumulation layer instead of an inversion layer at the *p*-type silicon surface, the above-mentioned parasitic shunting effect at the solar cell rear is not expected for an Al_2O_3 -rear-passivated cell. In combination with its very high transparency for near-bandgap photons, ALD-deposited Al_2O_3 should hence be an optimal choice for a dielectric layer at the silicon solar cell rear.

Note that on *n*-type silicon with a resistivity of ~ 2 Ωcm also very low SRVs of 4 cm/s have been measured over the entire relevant injection range [10,14]. Hence ALD- Al_2O_3 is also excellently suited for passivating the rear of *n*-type silicon solar cells. In Section 4 the potential of *all-Al_2O_3* passivated *n*-type cells will be analysed in detail.

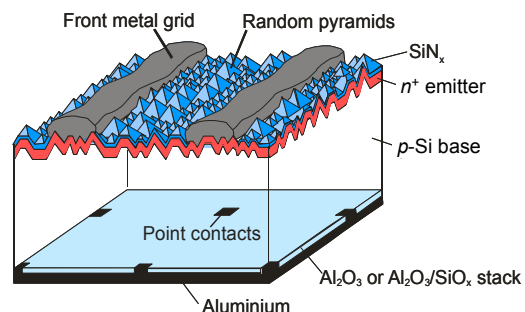


Figure 3. PERC-type solar cell structure used to demonstrate the applicability of an Al_2O_3 rear surface passivation to high-efficiency solar cells.

Table 1. One-sun parameters measured under standard testing conditions of 290 μm thick PERC-type silicon solar cells with three different rear surface passivations: (i) thermal SiO_2 (220 nm), (ii) ALD- Al_2O_3 (130 nm) and (iii) ALD- Al_2O_3 (30 nm)/PECVD- SiO_x (200 nm). All cells were fabricated on 0.5- Ωcm FZ p -Si wafers [11].

Rear side	Cell ID	V_{oc} [mV]	J_{sc} [mA/cm ²]	FF [%]	η [%]
Thermal SiO_2 (220 nm)	7_1	656	38.9	80.3	20.5
	Average of 4	655 \pm 1	38.4 \pm 0.5	80.3 \pm 1.3	20.2 \pm 0.3
ALD- Al_2O_3 (130 nm)	3_3	655	38.7	78.9	20.0*
	Average of 4	656 \pm 2	38.6 \pm 0.1	79.4 \pm 1.4	20.0 \pm 0.4
ALD- Al_2O_3 (30 nm)/ PECVD- SiO_x (200 nm)	2_4	660	39.0	80.1	20.6*
	Average of 8	657 \pm 2	38.6 \pm 0.3	80.4 \pm 1.1	20.4 \pm 0.4

*Calibrated measurement at Fraunhofer ISE CalLab.

Figure 3 shows the PERC-type solar cell structure used to demonstrate the applicability of Al_2O_3 rear surface passivation to high-efficiency silicon solar cells. The starting material is (100)-oriented boron-doped float-zone (FZ) silicon with a thickness of 310 μm and a resistivity of 0.5 Ωcm . After damage etching and wet chemical cleaning, an SiO_2 layer is grown on both wafer surfaces in a wet oxidation process at 1000°C. Subsequently, 2 \times 2 cm^2 diffusion windows are photolithographically opened on one wafer side and the silicon surface within the windows is textured with random pyramids in a KOH/isopropanol solution. A single-step phosphorus emitter is diffused from a POCl_3 source, resulting in an n^+ -emitter with a sheet resistance of 100 Ω/square , and the phosphorus glass is removed by a short HF dip. At this point of the process, the cell batch is split up into three batches, of which each one receives a different rear surface passivation: (i) one batch of cells keeps the thermally grown SiO_2 , (ii) the second one is coated by a 130 nm Al_2O_3 film and (iii) the third batch is passivated by a stack consisting of a 30 nm Al_2O_3 layer and a 200 nm thick PECVD- SiO_x layer. The Al_2O_3 films are deposited by plasma-assisted ALD at a deposition temperature of 200°C. The plasma-assisted ALD Al_2O_3 process is split up into two self-limiting reactions consisting of a trimethyl-aluminum [$\text{Al}(\text{CH}_3)_3$] exposure and an O_2 plasma. The subsequent annealing step as applied in the study of Hoex et al. [10] is omitted in this case as adequate post-deposition annealing steps are already present in the cell process (tunnel oxidation at 500°C). The SiO_x layer is deposited in a continuous PECVD process using silane (SiH_4) and nitrous oxide (N_2O) as process gases. The remaining process steps are identical for all three cell batches. Using photolithography point contact openings are etched into the dielectric layers at the rear. A photolithography mask resulting in a point contact pitch of 2 mm and a metallization fraction of 4% is used. 20 μm of Aluminium is evaporated on the entire cell rear using electron-beam evaporation. A tunnel oxidation of the n^+ -emitter is performed at 500°C for 10 min, resulting in an \sim 1.5 nm thick oxide layer [15]. The 20 μm thick Al front metal grid is then evaporated through a shadow mask onto the tunnel oxide. Finally, a surface-passivating SiN_x antireflection coating is deposited onto the front of the PERC solar cell by remote-PECVD at 300°C. The

aperture area of all solar cells is 4 cm^2 and the entire front metallization, including the busbar, is within the active cell area.

Table 1 summarizes the one-sun parameters of the processed PERC-type solar cells featuring different rear surface passivation schemes, as measured under standard testing conditions (25°C, 100 mW/cm^2 , AM 1.5 G). The results marked with an asterisk were independently confirmed at Fraunhofer ISE CalLab. The best reference solar cell with alnealed SiO_2 rear surface passivation is characterized by an efficiency of $\eta = 20.5\%$, an open-circuit voltage of $V_{oc} = 656$ mV and a short-circuit current density of $J_{sc} = 38.9$ mA/cm^2 . The analysis of the internal quantum efficiency (IQE) shows that the V_{oc} is limited by the front emitter. The average values of all 4 cells with SiO_2 rear passivation show only a very small scatter, demonstrating the high reproducibility of the process. The average parameters of the cells with Al_2O_3 , $\text{Al}_2\text{O}_3/\text{SiO}_x$ and SiO_2 rear passivation agree within the scatter ranges. In particular it is noticeable that the J_{sc} of the cells with Al_2O_3 and $\text{Al}_2\text{O}_3/\text{SiO}_x$ rear surface passivation is not reduced compared to the SiO_2 -passivated cells. In the case of high-positive-charge dielectrics, such as SiN_x with fixed positive charge densities $>10^{12}$ cm^{-2} , it was reported that J_{sc} is reduced by 1-2 mA/cm^2 compared to the thermal SiO_2 reference, due to the above-described parasitic shunting effect [6,7]. This effect is not expected in the case of Al_2O_3 as it is a negative-charge-dielectric inducing an accumulation layer. The cell results summarized in Table 1 confirm the expected non-existence of the parasitic shunting for Al_2O_3 -passivated as well as for $\text{Al}_2\text{O}_3/\text{SiO}_x$ -passivated rear surfaces. The best cell of the entire batch is obtained for the $\text{Al}_2\text{O}_3/\text{SiO}_x$ -passivated cell, resulting in an independently confirmed efficiency of $\eta = 20.6\%$, a V_{oc} of 660 mV and a J_{sc} of 39.0 mA/cm^2 .

It is not possible to quantify the exact rear surface passivation quality from comparison of the cell parameters given in Table 1, as these solar cells are largely limited by recombination losses in the front emitter. Hence, we analyze the IQE in the wavelength range 800-1200 nm to determine the rear SRVs of the different rear surface passivation schemes. The symbols in Fig. 4 show the IQE as a function of wavelength λ of PERC cells

Table 2. Effective rear surface recombination velocity S_r and internal rear reflectance R_r extracted from the IQE measurements shown in Fig. 5.

Rear side	Rear surface recombination velocity S_r [cm/s]	Internal rear reflectance R_r [%]
Thermal SiO ₂ (220 nm)	90 ± 20	91 ± 1
Al ₂ O ₃ (130 nm)	90 ± 20	90 ± 1
Al ₂ O ₃ (30 nm)/SiO _x (200 nm)	70 ± 20	91 ± 1

with the three different rear passivation schemes, measured at a fixed bias light intensity of 0.3 suns. The solid lines in Fig. 4 show the fits to the measured data. To model the $IQE(\lambda)$ dependence we use the software LAS-SIE [16,17], which combines the extended IQE evaluation by Basore [18] with the improved optical model developed by Brendel [19]. The bulk lifetime is assumed to be limited by Auger recombination, resulting in a bulk diffusion length of $L_b = 1500 \mu\text{m}$ for the 0.5 Ωcm p -type silicon material used in this work [20]. As we assume the intrinsic upper limit for the bulk lifetime, the SRVs determined from the IQE analysis are upper limits as well. Table 2 summarizes the rear SRVs S_r and the internal rear reflectances R_r extracted from the IQE analysis. All three rear structures are equally effective reflectors for near-bandgap photons ($R_r = 91\%$). The rear SRV (including recombination at the metal contacts) of the reference cell with annealed SiO₂ amounts to $S_r = (90 \pm 20)$ cm/s. The extracted S_r for the cell with single-layer Al₂O₃ rear passivation is the same as for the SiO₂-passivated reference cell, showing that ALD-deposited Al₂O₃ performs as good as aluminium-annealed high-temperature-grown SiO₂. A further reduction in the S_r is obtained for the Al₂O₃/SiO_x stack, resulting in an S_r of only (70 ± 20) cm/s, which we attribute to the hydrogenation of interface states at the Al₂O₃/Si interface during deposition of the hydrogen-rich SiO_x layer.

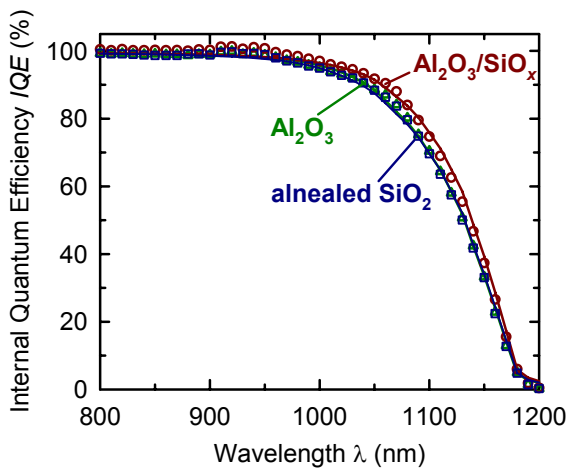


Figure 4. Measured internal quantum efficiency IQE as a function of wavelength λ (symbols) for solar cells with three different rear surface passivations: (i) thermal SiO₂ (220 nm), (ii) ALD-Al₂O₃ (130 nm) and (iii) ALD-Al₂O₃(30 nm)/PECVD-SiO_x(200 nm). The lines show the fitted $IQE(\lambda)$ curves. All measurements were taken with a white bias light intensity of ~ 0.3 suns [11].

The effective SRV of a point-contacted rear is given by Fischer's equation [17]

$$S_r = \frac{D_n}{W} \left[\frac{p}{2W\sqrt{\pi f}} \arctan\left(\frac{2W}{p} \sqrt{\frac{\pi}{f}}\right) - \exp\left(-\frac{W}{p}\right) + \frac{D_n}{fWS_{met}} \right]^{-1} + \frac{S_{pass}}{1-f}, \quad (1)$$

where D_n is the electron diffusion coefficient, W the wafer thickness, p the contact pitch, f the metallization fraction and S_{met} and S_{pass} are the SRVs on the metallized and on the passivated areas of the rear. According to Eqn. (1) the minimum SRV $S_{r,min}$ for a point-contact rear with perfect passivation in the non-metallized area (i.e., $S_{pass} = 0$) is given by the first summand on the right-hand side of Eqn. (1). For our cell structure we determine $S_{r,min} = 73$ cm/s ($D_n = 23 \text{ cm}^2/\text{s}$, $W = 290 \mu\text{m}$, $p = 2000 \mu\text{m}$, $f = 4\%$, $S_{met} \geq 10^5 \text{ cm/s}$). As the S_r of (70 ± 20) cm/s extracted from the IQE analysis is practically identical to the $S_{r,min}$ calculated using Eq. (1), we conclude that recombination in the passivated area of the cell rear can be completely neglected. Note that, although a slightly better passivation is obtained in the case of the Al₂O₃/SiO_x stacks, the rear SRV of the single-layer Al₂O₃-passivated cells is also mainly determined by recombination at the metal contacts. The IQE results clearly prove that atomic-layer-deposited Al₂O₃ is a very effective new dielectric passivation layer for high-efficiency silicon solar cells.

3 PASSIVATION OF B-DOPED p^+ EMITTERS

Emitter saturation current densities J_{0e} of boron-doped p^+ emitters were extracted from QSSPC measurements of the effective lifetime as a function of the injection density using the method of Kane and Swanson [21,12]. High-resistivity (20-90 Ωcm) shiny-etched n -type silicon wafers with a thickness of $\sim 260 \mu\text{m}$ were used as base material. BBr₃ diffusions were performed on both sides of the wafers in the temperature range 895-1010°C [22]. After etching off the boron glass, the drive-in was performed by a thermal oxidation at 1050°C [22]. All oxide-passivated samples received a 40-min forming gas anneal at 400°C before the QSSPC measurements. The sheet resistance of the p^+ emitters was determined from four-point probe measurements [23].

Figure 5 shows the measured emitter saturation current densities J_{0e} of the boron-diffused p^+ emitters as a function of their sheet resistance. After boron diffusion all samples were thermally oxidized and forming gas annealed. The open blue triangles in Fig. 5 show the result-

ing J_{0e} values ranging from 85 fA/cm² at a sheet resistance of 30 Ω/sq down to only 30 fA/cm² at 100 Ω/sq. However, as has been shown in a recent study [24], this very good passivation quality is highly unstable and after approximately two years of storage in the dark the J_{0e} of the oxide-passivated p^+ emitters degraded to ~300 fA/cm² (filled blue triangles in Fig. 5). The fact that SiO₂-passivated boron-doped p^+ emitters are unstable has also been observed on high-efficiency n -type PERL silicon solar cells with p^+ front emitter [25].

A very elegant method to improve the poor passivation quality of thermally grown SiO₂ on p^+ emitters has recently been proposed [26,27]. This method makes use of the excellent passivation quality of SiO₂ on n^+ surfaces by implementing an additional phosphorus diffusion at the surface of the p^+ emitter. The resulting n^+/p^+ junction at the surface can be well passivated as the excellent passivation properties of oxide on the n^+ surface are exploited. The described new passivation method has already been applied in the “buried emitter solar cell” [26,28] currently under development at ISFH.

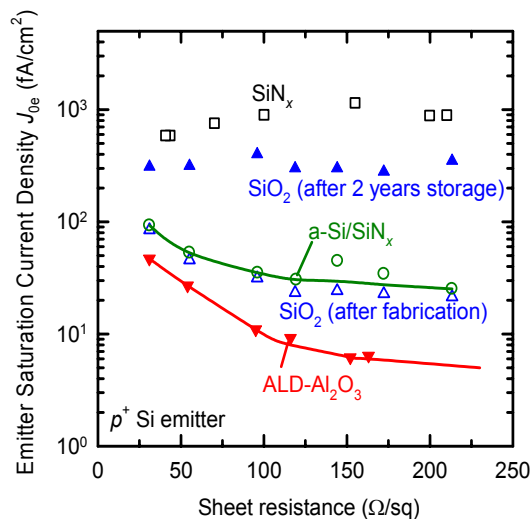


Figure 5. Measured emitter saturation current density J_{0e} of B-diffused p^+ emitters as a function of sheet resistance. Surfaces are passivated by (i) forming-gas-annealed thermal SiO₂ (open blue triangles), (ii) thermal SiO₂ after 2 years of storage in the dark (closed blue triangles), (iii) PECVD-SiN_x (open squares), (iv) a-Si/SiN_x stacks deposited by PECVD (open circles) [24] and (v) ALD-Al₂O₃ [12].

The black open squares in Fig. 5 show the J_{0e} values measured after stripping off the SiO₂ and depositing PECVD-SiN_x optimized for surface passivation on undiffused p -type silicon [29]. SiN_x gives by far the worst passivation quality of all investigated passivation schemes on p^+ emitters, which can partly be attributed to the large positive fixed charge density within the SiN_x films. However, it should also be mentioned here that a firing has recently been shown to improve the SiN_x passivation quality on boron-doped p^+ emitters [30]. The above-mentioned surface inversion method [26,27] of the p^+ emitter can also be applied in combination with SiN_x instead of thermal SiO₂ to improve the passivation quality

of the SiN_x on p^+ emitters. After etching off the SiN_x films the samples shown in Fig. 5 were passivated by double layers consisting of a 10 nm thick a-Si film deposited at 230°C and a 60 nm thick SiN_x layer deposited at the same temperature. The a-Si/SiN_x stacks were subsequently annealed at 350°C for 5 min to improve their passivation quality [24]. Despite the remarkably low deposition temperature, the a-Si/SiN_x stack passivates as effectively as the best high-temperature SiO₂ and is also perfectly stable, as has been shown in a recent study [24]. The main disadvantage of the a-Si/SiN_x stack regarding the application to the front p^+ emitter is the increased absorption within the a-Si layer, reducing the short-circuit density of the solar cell.

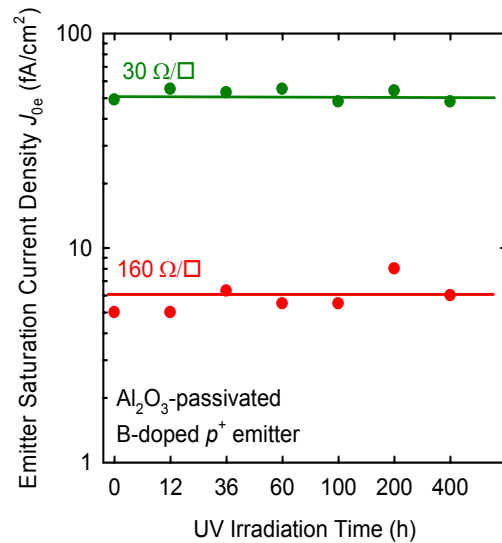


Figure 6. Perfect stability of Al₂O₃-passivated B-doped p^+ emitters under UV illumination. The experiments mimic 2 years outdoor conditions.

The filled red triangles in Fig. 5 show the measured J_{0e} values after stripping off the a-Si/SiN_x stacks, depositing Al₂O₃ by plasma-assisted ALD at 200°C and annealing the samples for 30 min at 425°C [12]. The J_{0e} values of the Al₂O₃-passivated p^+ emitters range from ~50 fA/cm² measured at a sheet resistance of 30 Ω/sq down to only 6 fA/cm² at 150 Ω/sq [12]. To our knowledge this is the best passivation realized so far on boron-doped p^+ emitters. A very high open-circuit voltage of 704 mV and an efficiency of 23.2% have in fact recently been realized using the above ALD-Al₂O₃ passivation scheme on the front boron-doped p^+ emitter of an n -type cell, whereas the rear was thermally oxidised [31]. As an additional advantage, Al₂O₃ as a large-bandgap material (~9 eV) is perfectly transparent for solar radiation. Hence, double layers of a thin (up to ~10 nm) Al₂O₃ film and a SiN_x antireflection layer on top are excellently suited for the application to high-efficiency cells on n -type silicon with a boron-doped p^+ front emitter.

We have also studied the stability of the Al₂O₃ passivation under UV illumination. The samples are kept under the same conditions as PV modules, i.e., they are positioned under a glass and an EVA sheet. 400 hours of UV exposure mimics the integrated amount of UV light the cells are exposed to during 2 years under average

outdoor conditions. The results of this experiment are shown in Fig. 6. The Al_2O_3 passivation is found to be perfectly stable and shows no degradation at all during UV exposure.

4 ALL- Al_2O_3 PASSIVATED CELLS

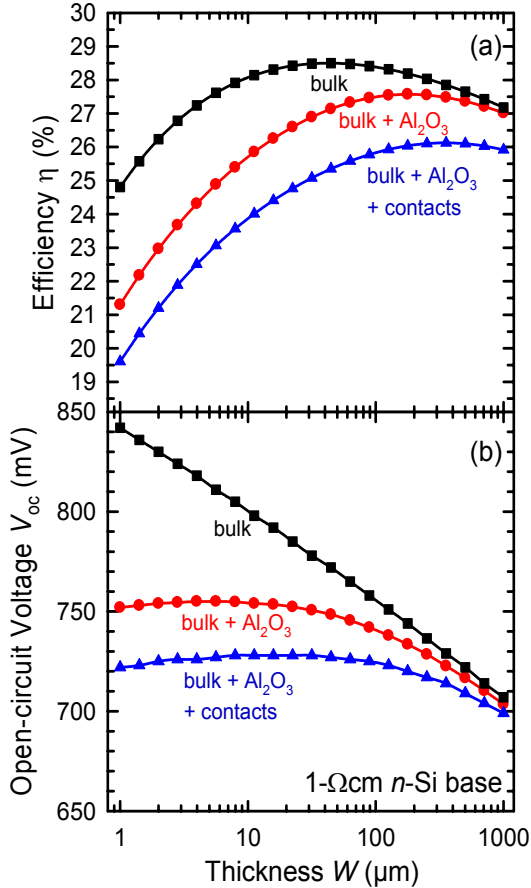


Figure 7. Calculated limiting (a) 1-sun efficiency η and (b) open-circuit voltage V_{oc} as a function of cell thickness W for a 1- Ωcm n -type silicon base assuming Lambertian light trapping. Black squares: only bulk recombination via Coulomb-enhanced Auger; red circles: additional surface recombination at the Al_2O_3 -passivated p^+ emitter and Al_2O_3 -passivated n -Si base; blue triangles: additional contact recombination and front-grid shading.

Using the measured recombination parameters of Al_2O_3 -passivated p^+ emitters and on undiffused Al_2O_3 -passivated n -type Si surfaces we calculate the 1-sun efficiency and V_{oc} limits for *all- Al_2O_3* passivated n -type silicon solar cells. For these calculations we assume an n -type silicon wafer with a base resistivity of 1 Ωcm and Lambertian light trapping [32]. The I - V characteristics is calculated using the expression

$$J = J_L - qW \frac{\Delta n}{\tau_b} - J_{0e} \left[\exp\left(\frac{qV}{kT}\right) - 1 \right] - qS_r \Delta n, \quad (2)$$

where J_L is the light-generated current density, W the cell thickness, τ_b the bulk lifetime, J_{0e} the emitter saturation current density and S_r the rear surface recombination velocity. In order to estimate the ultimate efficiency limit

for a 1-sun silicon solar cell we assume a perfectly passivated emitter and rear surface, i.e. $J_{0e} = 0$ and $S_r = 0$ in Eq. (2). The cell thickness W is varied between 1 and 1000 μm . The bulk recombination lifetime τ_b is assumed to be limited by Coulomb-enhanced Auger recombination, and we use a widely accepted parameterization as a function of the carrier densities [33].

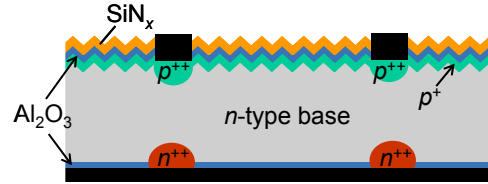


Figure 8. The *all- Al_2O_3* passivated n -type silicon solar cell has an efficiency limit of 26.1% including bulk, surface and contact recombination as well as shading losses.

Table 3. Calculated limiting 1-sun efficiency η and open-circuit voltage V_{oc} as a function of cell thickness W for a 1- Ωcm n -type silicon base assuming Lambertian light trapping.

Losses	η_{\max} (%)	V_{oc} @ η_{\max} (mV)
bulk	28.5	770
bulk + Al_2O_3	27.5	740
bulk + Al_2O_3 + contacts	26.1	720

Figure 7 and Table 3 show the calculated efficiency limit and the corresponding V_{oc} for three different cases. The uppermost curve (black squares) shows that Coulomb-enhanced Auger recombination limits the efficiency of a silicon solar cell to an ultimate efficiency of 28.5% for a cell thickness of ~ 50 μm . The red curve (circles) includes recombination in the Al_2O_3 -passivated boron-diffused p^+ emitter as well as recombination at the undiffused Al_2O_3 -passivated cell rear. For Al_2O_3 -passivated p^+ emitters we have measured a J_{0e} value of 6 fA/cm^2 and for undiffused n -type silicon a SRV of $S_r = 4$ cm/s . These additional recombination channels reduce the efficiency limit to 27.5% for a cell thickness between 100 and 300 μm . Moreover, the *all- Al_2O_3* passivated cell permits open-circuit voltages of up to 755 mV for a cell thickness between 3 and 10 μm . The V_{oc} limit drops to 740 mV at a cell thickness of 100 μm , where the efficiency peaks. Adding contact recombination and contact shading in a realistic way reduces the efficiency limit further to 26.1% and the V_{oc} limit to 728 mV (blue triangles in Fig. 7). **At a cell thickness of 200 μm our calculation gives a maximum efficiency of 26.1% at a V_{oc} of 720 mV.** The latter case corresponds to the cell structure shown in Fig. 8. Under the contacts we assume that heavy diffusions reduce the contact recombination. The front p^+ diffusion beneath the metal contacts has a sheet resistance of 5 Ω/sq , resulting in an emitter saturation current density of $J_{0e,\text{met}} = 420$ fA/cm^2 [34]. The n^+ diffusion at the rear has a sheet resistance of 30 Ω/sq and a

$J_{0r,met}$ of 350 fA/cm² [35], which corresponds to an $S_{r,met}$ of 150 cm/s. We use Eqn. (1) to determine the total rear SRV S_r as a function of cell thickness. For the metallization fraction at the front and the rear we assume a value of $f=3\%$. We also account for the optical shading losses by reducing J_L by 3%. Our calculations clearly show that due to the excellent level of surface passivation, a reduction of the contact recombination remains the major challenge in order to reach highest efficiencies.

5 CONCLUSIONS

Atomic layer deposition (ALD) of Al₂O₃ has been identified as an ideal new passivation scheme for passivating undiffused *p*- and *n*-type silicon surfaces as well as for the passivation of boron-doped *p*⁺ regions. Our calculations of efficiency and V_{oc} limits of *n*-type Si solar cells show that *all*-Al₂O₃ passivated cells have an efficiency limit of 27.5% at a V_{oc} of 740 mV. Including contact recombination and optical shading with realistic assumptions the efficiency limit drops to 26.1% at a V_{oc} of 720 mV.

In addition to the outstanding surface passivation provided by ALD-deposited Al₂O₃, the deposition process itself is also beneficial from an application point of view. In contrast to the conventionally applied PECVD, ALD consists of two self-limiting half-reactions, which implies several important advantages: (i) ALD gives highly conformal coatings, which allows to deposit and passivate e.g. deep trenches or even pores in silicon, (ii) pin-hole and particle-free deposition is achieved, (iii) as ALD is a self-limiting process uniform films can be deposited over large areas with mono-layer growth control and (iv) very low impurity concentrations of deposited films and hence very high film quality is achieved. The main disadvantage of ALD for photovoltaic applications is its relatively low deposition rate. However, this disadvantage can be overcome by depositing ultrathin (2-30 nm) ALD-Al₂O₃ films and capping them with a thicker film of e.g. PECVD-SiO_x, SiN_x or SiC_x [36]. Apart of the advantageous optical properties of these stacks, we have demonstrated that the passivation quality of such ALD/PECVD stacks can even be superior to that of single layers of Al₂O₃ [11], which we attribute to the hydrogenation of interface states at the Al₂O₃/Si interface during deposition of the hydrogen-rich PECVD layer. Combination of ALD and PECVD might hence be a key technology for future industrial high-efficiency solar cells.

ACKNOWLEDGEMENTS

The authors thank all members of the PV department at ISFH for their contributions to this work. Funding was provided by the State of Lower Saxony and the German Ministry for the Environment, Nature Conservation and Nuclear Safety (BMU).

REFERENCES

[1] J. Zhao, A. Wang, M.A. Green, *Prog. Photovolt.* **7**, 471 (1999).

- [2] M.J. Kerr, A. Cuevas, *Sem. Sci. Techn.* **17**, 35 (2001).
- [3] M.J. Stocks, A. Cuevas, A.W. Blakers, *Proc. 14th EUPVSEC*, Barcelona, Spain (1997), p. 770.
- [4] T. Lauinger, J. Schmidt, A.G. Aberle, R. Hezel, *Appl. Phys. Lett.* **68**, 1232 (1996).
- [5] J. Schmidt, J.D. Moschner, J. Henze, S. Dauwe, R. Hezel, *Proc. 19th EUPVSEC*, Paris, France (2004), p. 391.
- [6] S. Dauwe, L. Mittelstädt, A. Metz, J. Schmidt, R. Hezel, *Proc. 3rd WCPEC*, Osaka, Japan (2003), p. 1395.
- [7] S. Dauwe, L. Mittelstädt, A. Metz, R. Hezel, *Progr. Photovolt.* **10**, 271 (2002).
- [8] S. Dauwe, J. Schmidt, R. Hezel, *Proc. 29th IEEE PVSEC*, New Orleans, USA (2002), p. 1246.
- [9] G. Agostinelli, A. Delabie, P. Vitanov, Z. Alexieva, H.F.W. Dekkers, S. De Wolf, G. Beaucarne, *Sol. En. Mat. Sol. Cells* **90**, 3438 (2006).
- [10] B. Hoex, S.B.S. Heil, E. Langereis, M.C.M. van de Sanden, W.M.M. Kessels, *Appl. Phys. Lett.* **89**, 042112 (2006).
- [11] J. Schmidt, A. Merkle, R. Brendel, B. Hoex, M.C.M. van de Sanden, W.M.M. Kessels, *Progr. Photovolt.* (2008), DOI: 10.1002/pip.823.
- [12] B. Hoex, J. Schmidt, R. Bock, P. P. Altermatt, M. C. M. van de Sanden, and W. M. M. Kessels, *Appl. Phys. Lett.* **91**, 112107 (2007).
- [13] S. Dauwe, Ph.D. thesis, ISFH, University of Hanover, Germany, 2003.
- [14] B. Hoex, J. Schmidt, P. Pohl, M.C.M. van de Sanden, W.M.M. Kessels, *J. Appl. Phys.*, in press.
- [15] R. Hezel and K. Jaeger, *J. Electrochem. Soc.* **136**, 518 (1989).
- [16] www.pv-tools.de
- [17] B. Fischer, Ph.D. thesis, Univ. Konstanz, 2003.
- [18] P.A. Basore, *Proc. 23rd IEEE PVSC* (1993), p. 147.
- [19] R. Brendel, R. Plieninger, *Techn. Digest 9th International PVSEC*, Miyazaki, Japan (1996), p. 521.
- [20] P.P. Altermatt, J. Schmidt, G. Heiser, A.G. Aberle, *J. Appl. Phys.* **82**, 4938 (1997).
- [21] D. E. Kane, R.M. Swanson, *Proc. 18th IEEE PVSC*, Las Vegas, USA (1985), p. 578.
- [22] M. Kerr, Ph.D. thesis, Australian National University, Australia, 2002.
- [23] R. Bock, P.P. Altermatt, J. Schmidt, this conf.
- [24] P.P. Altermatt H. Plagwitz, R. Bock, J. Schmidt, R. Brendel, M.J. Kerr, A. Cuevas, *Proc. 21st EUPVSEC*, Dresden, Germany (2006), p. 647.

- [25] J. Zhao, J. Schmidt, A. Wang, G. Zhang, B.S. Richards, M.A. Green, *Proc. 3rd WCPEC*, Osaka, Japan (2003), p. 923.
- [26] N.P. Harder, V. Mertens, R. Brendel, *phys. stat. sol. (RRL)* **2**, 148 (2008).
- [27] J. Benick, O. Schultz-Wittmann, J. Schön, S.W. Glunz, *phys. stat. sol. (RRL)* **2**, 145 (2008).
- [28] Patent pending, ISFH.
- [29] J. Schmidt, M.J. Kerr, *Solar Energy Materials and Solar Cells* **65**, 585 (2001).
- [30] F.W. Chen, T. Li, J.E. Cotter, *Appl. Phys. Lett.* **88**, 263514 (2006).
- [31] J. Benick, B. Hoex, O. Schultz, S. Glunz, *Proc. 33rd IEEE PVSC*, San Diego, USA (2008).
- [32] R. Brendel, *Thin-Film Crystalline Silicon Solar Cells*, Wiley-VCH (2003).
- [33] J. Schmidt, M. Kerr, P.P. Altermatt, *J. Appl. Phys.* **88**, 1494 (2000).
- [34] D. E. Swanson, R. Kane, *Proc. 18th IEEE PVSC*, Las Vegas, USA (1985), p. 578.
- [35] M. Kerr, Ph.D. thesis, Australian National University (2002).
- [36] J. Schmidt, A. Merkle, B. Hoex, M.C.M. van de Sanden, W.M.M. Kessels, R. Brendel, *Proc. 33rd IEEE PVSC*, San Diego, USA (2008).